Efficient PGD-based dynamic calculation of non-linear soil behavior

Claudia Germoso [a], Jose V. Aguado [b], Alberto Fraile [a], Enrique Alarcon [a], Francisco Chinesta [b],*

[a] School of Industrial Engineering (ETSII), Universidad Politécnica de Madrid (UPM), José Gutiérrez Abascal, 28006 Madrid, Spain
[b] Institut de recherche en génie civil et mécanique (GeM UMR CNRS 6183), Ecole centrale de Nantes, 1, rue de la Noe, BP 92101, 44321 Nantes cedex 3, France

A B S T R A C T

Non-linear behavior of soils during a seismic event has a predominant role in current site response analysis. Soil response analysis consistently indicates that the stress–strain relationship of soils is non-linear and shows hysteresis. When focusing on forced response simulations, time integrations based on modal analysis are widely considered; however, parametric analysis, non-linear behavior and complex damping functions make difficult the online use of standard discretization strategies, e.g., those based on the use of finite element. In this paper, we propose a new harmonic analysis formulation, able to address forced response simulation of soils exhibiting their characteristic non-linear behavior. The solution can be evaluated in real-time from the offline construction of a parametric solution to the associated linearized problem within the Proper Generalized Decomposition framework.

© 2015 Académie des sciences. Published by Elsevier Masson SAS. This is an open access article under the CC BY-NC-ND license (http://creativecommons.org/licenses/by-nc-nd/4.0/).

1. Introduction

It is well known that solid mechanics can be formulated either in the time or in the frequency domains. The first one is preferred when calculating transient responses, whereas the frequency approach is an appealing alternative when forced response simulations are envisaged. There are decades of intense work in both kind of descriptions [7]. The general discrete form of linear solid dynamics writes

$$\mathbf{M}\frac{d^2\mathbf{U}(t)}{dt^2} + \mathbf{C}\frac{d\mathbf{U}(t)}{dt} + \mathbf{K}\mathbf{U}(t) = \mathbf{F}(t) \tag{1}$$

where $\mathbf{M}$, $\mathbf{C}$ and $\mathbf{K}$ are respectively the mass, damping and stiffness matrices, $\mathbf{U}$ the vector that contains the nodal displacements and $\mathbf{F}$ the nodal excitations (forces).

The main drawback related to the time integration of Eq. (1) lies in the necessity of solving a linear system (usually of very large size) at each time step, in particular when some of these matrices change in time for a variety of reasons (time-dependent behavior, non-linearities...).

* Corresponding author.
E-mail addresses: claudia.germoso.nunez@alumnos.upm.es (C. Germoso), jose.aguado-lopez@ec-nantes.fr (J.V. Aguado), afraile@etsii.upm.es (A. Fraile), enrique.alarcon@upm.es (E. Alarcon), Francisco.Chinesta@ec-nantes.fr (F. Chinesta).

Loads can be easily expressed in the frequency domain. In what follows, we consider without loss of generality the simplest scenario: $\mathbf{F}(t) = \mathbf{f}g(t)$, with $\|\mathbf{f}\| = 1$. The time function $g(t)$ can be expressed from the superposition of harmonic functions $\mathrm{e}^{\mathrm{i}\omega t}$, with ω the circular frequency and $\mathrm{i} = \sqrt{-1}$. If we assume a single frequency harmonic excitation, $g(t) = \mathrm{e}^{\mathrm{i}\omega t}$, the response of a linear solid is expected to have the same frequency, but to exhibit a certain phase angle θ, i.e. $\mathbf{U}(t) = \overline{\mathbf{U}}\mathrm{e}^{\mathrm{i}\omega t + \mathrm{i}\theta}$, where $\overline{\mathbf{U}}$ is the vector containing the amplitude of the nodal displacements. This vector can be rewritten as $\mathbf{U}(t) = \overline{\mathbf{U}}\mathrm{e}^{\mathrm{i}\omega t + \mathrm{i}\theta} = \mathbb{U}\mathrm{e}^{\mathrm{i}\omega t}$, where now $\mathbb{U} = \overline{\mathbf{U}}\mathrm{e}^{\mathrm{i}\theta}$ denotes a vector of complex entries, with $\mathbb{U} = \mathbf{U}_r + \mathrm{i}\mathbf{U}_i$, where $\mathbf{U}_r$ and $\mathbf{U}_i$ are respectively the real and imaginary parts of $\mathbb{U}$.

By introducing $\mathbf{F}(t) = \mathbf{f}\mathrm{e}^{\mathrm{i}\omega t}$ and $\mathbf{U}(t) = \mathbb{U}\mathrm{e}^{\mathrm{i}\omega t}$ into Eq. (1), one has the frequency-based description of solid dynamics

$$\left(-\omega^2\mathbf{M} + \mathrm{i}\omega\mathbf{C} + \mathbf{K}\right)\mathbb{U} = \mathbf{f} \tag{2}$$

where the exponential factor $\mathrm{e}^{\mathrm{i}\omega t}$ was eliminated from both members.

Imagine for a while that damping vanishes, i.e. $\mathbf{C} = \mathbf{0}$, and that we focus on the free response of the mechanical system, i.e. $\mathbf{f} = \mathbf{0}$. In this case, Eq. (2) reduces to:

$$\mathbf{K}\mathbb{U} = \omega^2\mathbf{M}\mathbb{U} \tag{3}$$

which defines an eigenproblem that results in the eigenmodes $\mathbb{U}_i$ and the associated eigenfrequencies ω_i^2. Eigenmode $\mathbb{U}_i$ scaled from some normalization condition is called normal mode and is noted by $\boldsymbol{\phi}_i$. It is usual to normalize eigenmodes according to $\boldsymbol{\phi}_i^{\mathrm{T}}\mathbf{M}\boldsymbol{\phi}_i = M_i = 1$, from which it results $\boldsymbol{\phi}_i^{\mathrm{T}}\mathbf{K}\boldsymbol{\phi}_i = K_i = \omega_i^2$, where M_i and K_i are known as modal mass and modal stiffness, respectively. If normal modes are placed in the columns of matrix $\mathbf{P}$, we could express $\mathbb{U}$ in the orthonormal basis defined by the normal modes, according to

$$\mathbb{U} = \mathbf{P} \cdot \boldsymbol{\eta}(t) \tag{4}$$

Now, by injecting (4) into Eq. (1), premultiplying by the transpose of $\mathbf{P}$ and taking into account the orthogonality conditions $\boldsymbol{\phi}_j^{\mathrm{T}}\mathbf{M}\boldsymbol{\phi}_i = 0$ and $\boldsymbol{\phi}_j^{\mathrm{T}}\mathbf{K}\boldsymbol{\phi}_i = 0$ when $i \neq j$, it results

$$\mathbf{I}\frac{\mathrm{d}^2\boldsymbol{\eta}(t)}{\mathrm{d}t^2} + \mathbf{P}^{\mathrm{T}}\mathbf{C}\mathbf{P}\frac{\mathrm{d}\boldsymbol{\eta}(t)}{\mathrm{d}t} + \mathbf{diag}(\omega_i^2)\boldsymbol{\eta}(t) = \mathbf{P}^{\mathrm{T}}\mathbf{F}(t) \tag{5}$$

where $\mathbf{I}$ is the unit matrix.

When damping vanishes, $\mathbf{C} = \mathbf{0}$, the previous equation reduces to a linear system of uncoupled second-order ordinary differential equations.

When damping applies, matrix $\tilde{\mathbf{C}} \equiv \mathbf{P}^{\mathrm{T}}\mathbf{C}\mathbf{P}$ is not in general diagonal, compromising the efficiency of modal analysis. To circumvent this issue, different diagonalization procedures have been proposed and widely used. Two usual diagonalization procedures are: (i) diagonalization by model damping that expresses $\tilde{\mathbf{C}} = \mathbf{diag}(2\zeta_i\omega_i)$, where ζ_i denotes the damping ratio for the i-th natural mode; and (ii) Rayleigh diagonalization that by assuming $\mathbf{C} = a_0\mathbf{M} + a_1\mathbf{K}$ results in $\tilde{\mathbf{C}} = \mathbf{diag}(a_0 + a_1\omega_i^2) = \mathbf{diag}(2\zeta_i\omega_i)$, with $\zeta_i = \frac{1}{2}\left(\frac{a_0}{\omega_i} + a_1\omega_i\right)$. These choices imply approximations whose validity and accuracy must be checked. A more precise route consists in extracting the modes from the solution to the quadratic complex eigenproblem

$$\left(\mathbf{K} + \mathrm{i}\omega\mathbf{C} - \omega^2\mathbf{M}\right)\mathbb{U} = \mathbf{0} \tag{6}$$

However, many time models involve parametric damping, that is, damping depends on some parameters grouped in vector $\boldsymbol{\mu}$, $\mathbf{C}(\boldsymbol{\mu})$, and in that case the solution to parametric quadratic eigenproblems remains an open issue [16,18].

As we are interested in solving problems with parametric damping, as discussed later, we decide to renounce to direct time integrations and also to modal-analysis-based time integrations, in favor of an alternative approach, purely harmonic, making use of Eq. (2).

Imagine that the applied load can be written from the superposition of harmonic functions of angular frequency ω

$$g(t) = \int_{-\infty}^{\infty} c(\omega)\,\mathrm{e}^{\mathrm{i}\omega t}\mathrm{d}\omega \tag{7}$$

where $c(\omega)$ represents the content of each harmonic $\mathrm{e}^{\mathrm{i}\omega t}$ in $g(t)$. In fact, $c(\omega)$ is the Fourier transform of $g(t)$:

$$c(\omega) \equiv \mathcal{F}(g(t)) = \int_{-\infty}^{\infty} g(t)\,\mathrm{e}^{-\mathrm{i}\omega t}\mathrm{d}t \tag{8}$$

In general, $c(\omega < \omega^-) = c(\omega > \omega^+) \approx 0$, i.e.

$$g(t) \approx \int_{\omega^-}^{\omega^+} c(\omega) e^{i\omega t} \, d\omega \tag{9}$$

which implies that Eq. (2) must be solved for any value of $\omega \in [\omega^-, \omega^+]$

$$\left(-\omega^2 \mathbf{M} + i\omega \mathbf{C} + \mathbf{K}\right) \mathbb{U}(\omega) = \mathbf{f} \tag{10}$$

which leads to the parametric solution $\mathbb{U}(\omega)$, which, by applying the superposition principle that characterizes linear behaviors, leads to the general solution

$$\mathbf{U}(t) = \int_{\omega^-}^{\omega^+} c(\omega) \, \mathbb{U}(\omega) \, e^{i\omega t} \, d\omega \tag{11}$$

The main drawback of that approach is the necessity of solving a linear system related to the solution to Eq. (10) for each value of ω involved in the discrete inverse transform (11), number that increases with the frequency interval length $\Delta\omega = |\omega^+ - \omega^-|$ and with the resolution of the signal. For this reason, modal analysis is much more employed than harmonic analysis.

In the case of parametric models, mass, damping and stiffness matrices can depend on a series of parameters grouped in the vector $\boldsymbol{\mu}$, i.e. $\mathbf{M}(\boldsymbol{\mu})$, $\mathbf{C}(\boldsymbol{\mu})$ and $\mathbf{K}(\boldsymbol{\mu})$, making difficult, as indicated above, the use of modal analysis, which requires solving parametric eigenproblems [16,18]. On the other hand, the use of harmonic analysis requires solving Eq. (10) for each frequency ω and each possible choice of the parameters $\boldsymbol{\mu}_j$, $\mathbb{U}(\omega; \boldsymbol{\mu}_j)$ to finally compute the discrete sum related to

$$\mathbf{U}(t; \mu_j) = \int_{\omega^-}^{\omega^+} c(\omega) \, \mathbb{U}(\omega; \boldsymbol{\mu}_j) \, e^{i\omega t} \, d\omega \tag{12}$$

for any choice of the parameters $\boldsymbol{\mu}_j$.

Thus, if for example we consider two parameters $\boldsymbol{\mu}^{\mathrm{T}} = (\mu_1, \mu_2)$, each one sampled using hundred values, $\boldsymbol{\mu}_j$ involves 10^4 samples, i.e. $j = 1, \cdots, 10^4$. Now, if we assume 10^4 discrete frequencies involved in the reconstruction of $g(t)$, the calculation of the parametric solution $\mathcal{U}(\omega_i; \boldsymbol{\mu}_j)$ requires solving 10^8 linear systems.

The use of the Proper Generalized Decomposition largely considered in our former works [3–6], allows solving the parametric model

$$\left(-\omega^2 \mathbf{M}(\boldsymbol{\mu}) + i\omega \mathbf{C}(\boldsymbol{\mu}) + \mathbf{K}(\boldsymbol{\mu})\right) \mathbb{U}(\omega, \boldsymbol{\mu}) = \mathbf{f} \tag{13}$$

by assuming the separated representation

$$\mathbb{U}(\omega, \mu_1, \mu_2) \approx \sum_{k=1}^{N} \mathbf{Z}_k W_k(\omega) \mathcal{M}_k^1(\mu_1) \mathcal{M}_k^2(\mu_2) \tag{14}$$

where $\mathbf{Z}_k$ is a vector of nodal displacements and $W_k(\omega)$, $\mathcal{M}_k^1(\mu_1)$ and $\mathcal{M}_k^2(\mu_2)$ are functions that depend on the extra-coordinates ω, μ_1 and μ_2, respectively. The construction of the separated representation (14) implies the solution of a number of linear systems scaling with the number of terms involved in the finite sum, i.e. in the order of N linear systems (N being in general of few tens). When referring to soil models, the parameters are related to the strain–stress non-linear behavior, in fact to its linearized behavior as described later.

It is important to note that in soil mechanics [15], damping is also assumed scaling with frequency. The interested reader can refer to [8], where the theoretical consequences of assuming a frequency dependent dashpot parameter are analyzed. In [8], it was proved that even if such a choice succeeded to fit the experimental data, when coming back to the time space, causality is lost, and then the resulting expressions in the time domain were called *non-equations*. Anyway, it is important to note that even when considering complex non-linear frequency-dependent damping $\mathbf{C}(\omega)$ in Eq. (2), the problem in the frequency domain remains linear because here the frequency is a model parameter (or a model extra-coordinate within the PGD framework).

In what follows, and as previously indicated, we are considering particular non-linearities that only apply in the frequency domain. It is important to recall that as soon as a solid with a real non-linear behavior is excited with a load of a given frequency, the response can contain a large spectrum of frequencies. In the case of soils, when applying a load of a certain frequency, the response has the same frequency, however in the frequency space, the superposition principle fails to prove the existence of a non-linear behavior that depends on the strain amplitude [10,13,14]. This subtle issue will be revisited later.
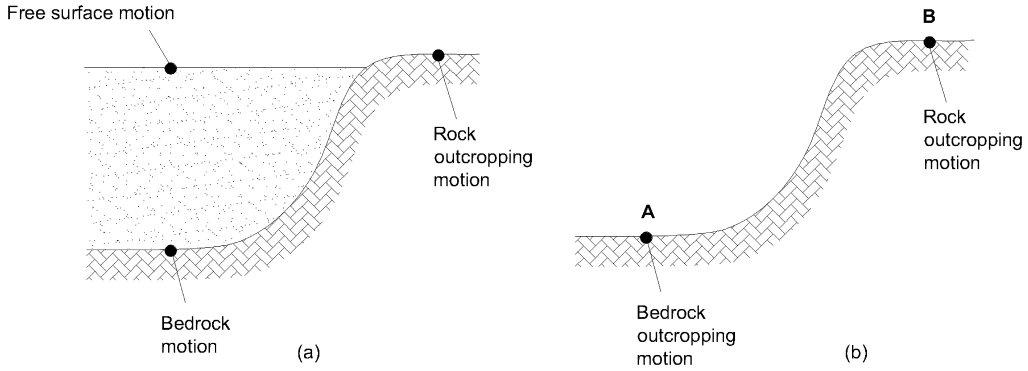
Fig. 1. Ground response representation: (a) bedrock motion; (b) bedrock outcropping motion.

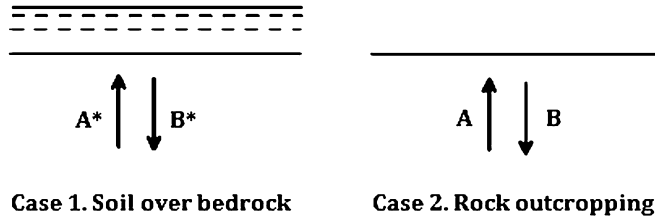**Case 1. Soil over bedrock**   **Case 2. Rock outcropping**

Fig. 2. Amplitudes of the incident and reflected waves in the soil over bedrock and rock outcropping.

After this introduction that served to justify the choice of a fully harmonic description, we describe in the next section the rock outcropping motion problem that allows deriving the boundary conditions to be applied in the soil dynamic problem described in Section 3. The linearization strategy will be described in Section 4 and then it will be efficiently discretized in Section 5 within the Proper Generalized Decomposition framework, leading to an efficient non-linear solver described in Section 6. Finally, Section 7 illustrates the potentiality of the proposed approach from some numerical examples.

2. The rock outcropping motion

In soil analysis, the control is defined from the response spectrum, or its corresponding time history, at bedrock by what is known as *rock outcropping motion* (Fig. 1b). From the outcropping motion, the objective is to predict the bedrock motion covered by the soil deposit (Fig. 1a). This problem was solved in [11] for the special case of a layered non-linear deposit overlying a uniform linearly elastic half-space.

Considering the schema in Fig. 2, the bedrock is located at the base of a soil column in Case 1 and as rock outcropping in Case 2. In the case of rock outcropping, the incident and reflected waves (A and B in Fig. 2) are equivalent; however, in the other case, the reflected waves (B^*) differ because some waves are transmitted to the soil deposit.

In Appendix A it is justified that in the base of the soil column the bedrock half-space can be replaced by a dashpot whose behavior is modeled by

$$\tau_0^* = \rho \, c_s \dot{U}_s - \rho \, c_s \dot{U}_0^* \tag{15}$$

where ρ is the bedrock density, c_s the wave velocity, $\dot{U}_s$ the rock outcropping velocity (assumed measurable) and $\dot{U}_0^*$ the velocity at the base of the soil column, that coincides with the soil-bedrock half-space interface and τ_0^* the shear stress at that position.

Thus, the bedrock half-space can be replaced by the boundary condition (15) that also includes the measured rock outcropping motion $\dot{U}_s$. In [11] this boundary condition was applied at the base of the soil deposit that was analyzed in the non-linear regime while taking into account the effects of the underlying bedrock half-space.

3. Wave equation for a linear soil deposit

The equation of linear dynamics in the case of a one-dimensional column reads:

$$\rho A \frac{\partial^2 u(z,t)}{\partial t^2} = G A \frac{\partial^2 u(z,t)}{\partial z^2} \tag{16}$$

where $u(z,t)$ is the displacement field, G is the shear modulus, ρ the density and A the area of the column. If a harmonic excitation of frequency ω applies, the solution to the shear wave propagation equation is also harmonic and of the same frequency, i.e. $u(z,t) = \mathcal{U}(z) \, e^{i\omega t}$. Thus it results

$$-\rho A \omega^2 \mathcal{U}(z) = G A \frac{\partial^2 \mathcal{U}(z)}{\partial z^2} \tag{17}$$

As previously discussed, for the purpose of modeling, the half-space is substituted by a viscous damper, that when considering a harmonic load of unit amplitude it results

$$G A \frac{\partial \mathcal{U}(z)}{\partial z}\Big|_{z=0} = 1 - c_s \, \rho \, A \, \mathrm{i} \, \omega \, U(0) \tag{18}$$

On the other hand, the stress-free condition at the free surface reads

$$G A \frac{\partial U(z)}{\partial z}\Big|_{z=L} = 0 \tag{19}$$

In the case of a simple harmonic motion, damping can conveniently be expressed by using the concept of complex stiffness. The equivalent linear model represents the soil's stress–strain response using a Kelvin–Voigt model. Thus, the shear stress τ depends on the shear strain γ and its rate $\dot{\gamma}$ according to

$$\tau = G \gamma + G' \frac{\mathrm{d}\gamma}{\mathrm{d}t} \tag{20}$$

or in the frequency domain as

$$\tau = (G + \mathrm{i}\omega G')\gamma \tag{21}$$

The complex shear modulus G^* reads

$$G^* = G + \mathrm{i}\omega G' = G(1 + \mathrm{i}2\zeta) \tag{22}$$

Observe in Eq. (22) G' scales with the inverse of frequency in such a manner that the complex shear modulus is now frequency-independent. We refer to Section 1 for a deeper discussion on the consequences of this choice. Introducing Eq. (22) into Eq. (17) it results:

$$\rho \omega^2 \mathcal{U}(z) + G^* \frac{\partial^2 \mathcal{U}(z)}{\partial z^2} = 0 \tag{23}$$

The weak formulation related to the equation (23) is obtained by considering a test function $\mathcal{U}^*$ defined in the domain $\Omega_z = (0, L)$, integrating by parts and considering the boundary conditions (18) and (19)

$$\int_{\Omega_z} \mathcal{U}^*(z)\rho \omega^2 \mathcal{U}(z)\,\mathrm{d}z - \int_{\Omega_z} \frac{\partial \mathcal{U}^*}{\partial z} G^* \frac{\partial \mathcal{U}(z)}{\partial z}\,\mathrm{d}z + \mathcal{U}^*(0)\mathrm{i}\rho c_s \omega \mathcal{U}(0) - \mathcal{U}^*(0) = 0 \tag{24}$$

or

$$\int_{\Omega_z} \mathcal{U}^*(z)\rho \omega^2 \mathcal{U}(z)\,\mathrm{d}z - \int_{\Omega_z} \frac{\partial \mathcal{U}^*}{\partial z} G(1 + \mathrm{i}2\zeta) \frac{\partial \mathcal{U}(z)}{\partial z}\,\mathrm{d}z + \mathcal{U}^*(0)\mathrm{i}\rho c_s \omega \mathcal{U}(0) - \mathcal{U}^*(0) = 0 \tag{25}$$

4. Non-linear modelling

The so-called *equivalent linear approximation* was introduced with the aim of improving constitutive laws of soils. It was implemented into the EERA (Equivalent-linear Earthquake Response Analysis) software [1], a recent implementation of the well-known concepts of equivalent linear earthquake site response analysis, starting from the same basic concepts as in SHAKE software [17]. The linear approximation considers the shear modulus G and the damping ratio ζ constant for each soil stratum and both dependent on the strain level [2]. Obviously, with both parameters depending on the strain, and the last at its turn depending on the parameters choice, the problem becomes non-linear and an iteration process is required for solving it.

The dependence of shear modulus and damping ratio on the effective strain is illustrated in the curves shown in Fig. 3 for sand and clay. The effective strain is given by $\gamma_{\mathrm{eff}} = \frac{2}{3}\gamma_{\max}$ ($\sim 66\%$ of the peak strain), with $\gamma_{\max} = \max(|\gamma(t)|)$.

When the strain varies significantly along the deposit deep, or when the soil deposit is composed of different strata of different materials, one must consider different layers to which different values of G and ζ are assigned, depending on the material and on the strain level.

In order to speed-up calculations, one could compute offline the parametric solution $\mathcal{U}(z, \omega, G, \zeta)$ for the soil deposit, assuming the same values of G and ζ everywhere in the soil domain. When the soil column is partitioned in $\mathcal{L}$ layers, in which both coefficients are assumed constant, the parametric solution writes $\mathcal{U}(z, \omega, G_1, \zeta_1, \cdots, G_{\mathcal{L}}, \zeta_{\mathcal{L}})$.

As soon as such parametric solutions are available, the non-linear problem can be solved in real time because no new calculation is needed; the non-linear solver only needs particularize online the parametric solution calculated offline. The iteration process is detailed later, but before, the obtention of these parametric solutions within the Proper Generalized Decomposition framework (that allows circumventing the curse of dimensionality that highly dimensional problems entail) is summarized.
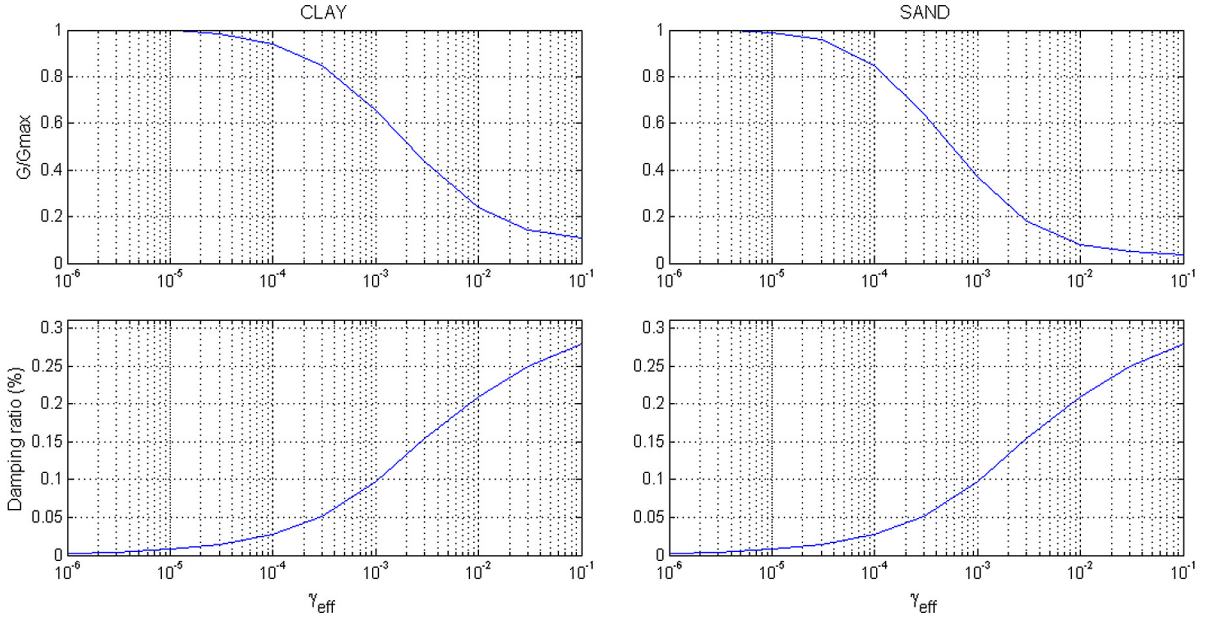
Fig. 3. Shear modulus ratio ($G/G_{\max}$) and damping ratio ζ for sand and clay.

5. Proper generalized decomposition-based parametric solutions

In this section, we describe the construction of the parametric solutions within the Proper Generalized Decomposition framework. For this purpose, we consider first the separated representation of the single-stratum parametric displacement:

$$\mathcal{U}(z, \omega, G, \zeta) \approx \sum_{i=1}^{N} Z_i(z) W_i(\omega) \mathcal{G}_i(G) \mathcal{E}_i(\zeta) \tag{26}$$

The PGD constructor widely described in [6,5] proceeds by calculating from $\mathcal{U}^n(z, \omega, G, \zeta)$, assumed already known that

$$\mathcal{U}^n(z, \omega, G, \zeta) = \sum_{i=1}^{n} Z_i(z) W_i(\omega) \mathcal{G}_i(G) \mathcal{E}_i(\zeta) \tag{27}$$

the new term of the finite sum, leading to the enriched approximate $\mathcal{U}^{n+1}(z, \omega, G, \zeta)$

$$\mathcal{U}^{n+1}(z, \omega, G, \zeta) = \sum_{i=1}^{n} Z_i(z) W_i(\omega) \mathcal{G}_i(G) \mathcal{E}_i(\zeta) + Z_{n+1}(z) W_{n+1}(\omega) \mathcal{G}_{n+1}(G) \mathcal{E}_{n+1}(\zeta) \tag{28}$$

In order to calculate functions $Z_{n+1}(z)$, $W_{n+1}(\omega)$, $\mathcal{G}_{n+1}(G)$ and $\mathcal{E}_{n+1}(\zeta)$, we proceed from the extended weak form

$$\int_{\Omega} \mathcal{U}^* \rho \omega^2 \mathcal{U} \, d\Omega - \int_{\Omega} \frac{\partial \mathcal{U}^*}{\partial z} G(1 + \mathrm{i}2\zeta) \frac{\partial \mathcal{U}}{\partial z} \, d\Omega + \mathcal{U}^*_{z=0} \mathrm{i} \rho c_s \omega \mathcal{U}_{z=0} - \mathcal{U}^*_{z=0} = 0 \tag{29}$$

where $\Omega = \Omega_z \times \Omega_\omega \times \Omega_G \times \Omega_\zeta$, with $\Omega_z = (0, L)$, $\Omega_\omega = (\omega^-, \omega^+)$, $\Omega_G = (G^-, G^+)$ and $\Omega_\zeta = (\zeta^-, \zeta^+)$ the domains in which the coordinates z, ω, G and ζ, respectively, are defined.

The four problems to be solved for calculating the four functions $Z_{n+1}(z)$, $W_{n+1}(\omega)$, $\mathcal{G}_{n+1}(G)$ and $\mathcal{E}_{n+1}(\zeta)$ are detailed in Sections B.1, B.2, B.3 and B.4 respectively, and summarized below.

(i) *Calculation of $Z_{n+1}(z)$.* With $\mathcal{U}^n(z, \omega, G, \zeta)$ known as well as $W_{n+1}(\omega)$, $\mathcal{G}_{n+1}(G)$ and $\mathcal{E}_{n+1}(\zeta)$ (randomly chosen at the first iteration or coming from the previous iteration of the non-linear solver), we introduce Eq. (28) into the weak form (29), where after integrating in $\Omega_\omega \times \Omega_G \times \Omega_\zeta$ the only unknown function is $Z_{n+1}(z)$. At this step, the test function $\mathcal{U}^*$ is chosen in the form

$$\mathcal{U}^* = Z^*(z) W_{n+1}(\omega) \mathcal{G}_{n+1}(G) \mathcal{E}_{n+1}(\zeta) \tag{30}$$

The resulting weak form is the one related to a second-order BVP (boundary value problem) whose discretization using an adequate technique leads to the searched function $Z_{n+1}(z)$:

$$\int\limits_{\Omega_z} Z^* \gamma_1 Z_{n+1} \, \mathrm{d}z - \int\limits_{\Omega_z} Z^{*'} \gamma_2 Z'_{n+1} \, \mathrm{d}z + \int\limits_{\Omega_z} Z^* \left(\sum_{i=1}^{i=n} \alpha_i Z_i + \beta_i Z''_i \right) \mathrm{d}z$$

$$+ Z^*(0) \sum_{i=1}^{i=n} \left(\beta_i Z'_i(0) + Z_i(0)\mathrm{i}\delta_i \right) - Z^*(0)\,\phi_1 + Z^*(0)\mathrm{i}\phi_2 Z_{n+1}(0) = 0 \tag{31}$$

where coefficients α_i, β_i, δ_i, γ_1, γ_2, ϕ_1 and ϕ_2 are the integrals in Ω_ω, Ω_G and Ω_ζ defined in Section B.1. By Z' and Z'' we denote the first and second derivatives of the univariate function Z, respectively. The previous weak form is discretized by using linear C^0 finite elements after integrating by parts the term in the third integral involving second derivatives. Another possibility consists in reconstructing the second derivative before performing that integral.

(ii) *Calculation of $W_{n+1}(\omega)$.* With $\mathcal{U}^n(z, \omega, G, \zeta)$ known as well as $Z_{n+1}(z)$ (the just obtained), $\mathcal{G}_{n+1}(G)$ and $\mathcal{E}_{n+1}(\zeta)$, Eq. (28) is introduced into the weak form (29) where after integrating in $\Omega_z \times \Omega_G \times \Omega_\zeta$ the only unknown function is now $W_{n+1}(\omega)$. At this step the test function $\mathcal{U}^*$ is chosen in the form

$$\mathcal{U}^* = Z_{n+1}(z)W^*(\omega)\mathcal{G}_{n+1}(G)\mathcal{E}_{n+1}(\zeta) \tag{32}$$

The resulting weak form is the one related to an algebraic problem whose discretization leads to the searched function $W_{n+1}(\omega)$:

$$\int\limits_{\Omega_\omega} W^* \left(\gamma_1 \omega^2 - \gamma_2 + \mathrm{i}\omega\phi_2 Z_{n+1}^2(0) \right) W_{n+1} \, \mathrm{d}\omega$$

$$+ \int\limits_{\Omega_\omega} W^* \left[-\phi_1 Z_{n+1}(0) + \sum_{i=1}^{i=n} (\alpha_i \omega^2 - \beta_i + \mathrm{i}\omega Z_i(0)Z_{n+1}(0)\delta_i)W_i \right] \mathrm{d}\omega = 0 \tag{33}$$

where coefficients α_i, β_i, δ_i, γ_1, γ_2, ϕ_1 and ϕ_2 are the integrals in $\Omega_z \times \Omega_G \times \Omega_\zeta$ defined in Section B.2.

(iii) *Calculation of $\mathcal{G}_{n+1}(G)$.* With $\mathcal{U}^n(z, \omega, G, \zeta)$ known as well as $Z_{n+1}(z)$ and $W_{n+1}(\omega)$ (the just updated) and $\mathcal{E}_{n+1}(\zeta)$, Eq. (28) is introduced into the weak form (29), where after integrating in $\Omega_z \times \Omega_\omega \times \Omega_\zeta$, the only unknown function now is $\mathcal{G}_{n+1}(G)$. At this step, the test function $\mathcal{U}^*$ is chosen in the form

$$\mathcal{U}^* = Z_{n+1}(z)W_{n+1}(\omega)\mathcal{G}^*(G)\mathcal{E}_{n+1}(\zeta) \tag{34}$$

The resulting weak form is the one related to an algebraic problem whose discretization leads to the searched function $\mathcal{G}_{n+1}(G)$:

$$\int\limits_{\Omega_G} \mathcal{G}^* \left(\gamma_1 - G\gamma_2 + \mathrm{i}\phi_2 Z_{n+1}^2(0) \right) \mathcal{G}_{n+1} \, \mathrm{d}G$$

$$+ \int\limits_{\Omega_G} \mathcal{G}^* \left[-\phi_1 Z_{n+1}(0) + \sum_{i=1}^{i=n} (\alpha_i - \beta_i G + \mathrm{i}Z_i(0)Z_{n+1}(0)\delta_i)\,\mathcal{G}_i \right] \mathrm{d}G = 0 \tag{35}$$

where coefficients α_i, β_i, δ_i, γ_1, γ_2, ϕ_1 and ϕ_2 are the integrals in $\Omega_z \times \Omega_\omega \times \Omega_\zeta$ defined in Section B.3.

(iv) *Calculation of $\mathcal{E}_{n+1}(\zeta)$.* With $\mathcal{U}^n(z, \omega, G, \zeta)$ known as well as $Z_{n+1}(z)$, $W_{n+1}(\omega)$ and $\mathcal{G}_{n+1}(G)$, all them just updated, Eq. (28) is injected into the weak form (29) where after integrating in $\Omega_z \times \Omega_\omega \times \Omega_G$ the only unknown function is now $\mathcal{E}_{n+1}(\zeta)$. At this step, the test function $\mathcal{U}^*$ is chosen in the form

$$\mathcal{U}^* = Z_{n+1}(z)W_{n+1}(\omega)\mathcal{G}_{n+1}(G)\mathcal{E}^*(\zeta) \tag{36}$$

The resulting weak form is the one related to an algebraic problem whose discretization leads to the searched function $\mathcal{E}_{n+1}(\zeta)$:

$$\int\limits_{\Omega_\zeta} \mathcal{E}^* \left(\gamma_1 - (1 + \mathrm{i}2\zeta)\gamma_2 + \mathrm{i}\phi_2 Z_{n+1}^2(0) \right) \mathcal{E}_{n+1} \, \mathrm{d}\zeta$$

$$+ \int\limits_{\Omega_\zeta} \mathcal{E}^* \left[-\phi_1 Z_{n+1}(0) + \sum_{i=1}^{i=n} (\alpha_i - \beta_i(1 + \mathrm{i}2\zeta) + \mathrm{i}Z_i(0)Z_{n+1}(0)\delta_i)\mathcal{E}_i \right] \mathrm{d}\zeta = 0 \tag{37}$$

where coefficients α_i, β_i, δ_i, γ_1, γ_2, ϕ_1 and ϕ_2 are the integrals in $\Omega_z \times \Omega_\omega \times \Omega_G$ defined in Section B.4.

(v) *Checking convergence.* Functions $Z_{n+1}(z)$, $W_{n+1}(\omega)$, $\mathcal{G}_{n+1}(G)$ and $\mathcal{E}_{n+1}(\zeta)$ are compared with the ones existing before the just four updates. If the difference is not small enough the previous four updates are performed again. When the difference becomes small enough, the procedure looks for the new approximate form $\mathcal{U}^{n+2}(z, \omega, G, \zeta)$ resulting from the just computed approximation $\mathcal{U}^{n+1}(z, \omega, G, \zeta)$.
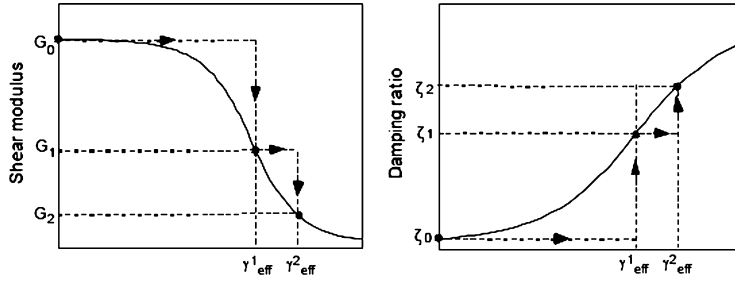
Fig. 4. Iteration process for determining the shear modulus G and damping ratio ζ as a function of the effective shear strain.

5.1. Parametric solution for stratified soil deposits

In the previous discussion, the properties of the material were assumed constant in the whole soil stratum. In this section, the soil deposit is assumed composed of $\mathcal{L}$ layers $\mathcal{D}_l$, $l = 1, \cdots, \mathcal{L}$, in which the properties are assumed constant (these different properties are related to the consideration of different materials, different strain levels implying different behavior in the non-linear case, or a combination of both factors).

Each layer is identified from its characteristic function $\chi_l(z)$, $l = 1, \cdots, \mathcal{L}$, defined as

$$\chi_l(z) = \begin{cases} 1 & \text{if } z \in \mathcal{D}_l \\ 0 & \text{if } z \notin \mathcal{D}_l \end{cases} \tag{38}$$

The resulting weak form reads now

$$\int_\Omega \mathcal{U}^*(z) \rho \omega^2 \mathcal{U}(z) \, \mathrm{d}\Omega - \int_\Omega \frac{\partial \mathcal{U}^*}{\partial z} (G_1^* \chi_1 + G_2^* \chi_2 + \cdots + G_\mathcal{L}^* \chi_\mathcal{L}) \frac{\partial \mathcal{U}(z)}{\partial z} \, \mathrm{d}\Omega + \mathcal{U}^*(0) \mathrm{i} \rho c_s \omega \mathcal{U}(0) - \mathcal{U}^*(0) = 0 \tag{39}$$

where

$$G_l^* = G_l(1 + \mathrm{i}2\zeta_l) \tag{40}$$

The parametric solution involves now the physical coordinate z, the frequency ω and the shear modulus and damping rate of each layer, G_l and ζ_l, $l = 1, \cdots, \mathcal{L}$:

$$\mathcal{U}(z, \omega, G_1, \zeta_1, G_2, \zeta_2, \cdots, G_\mathcal{L}, \zeta_\mathcal{L}) \approx \sum_{i=1}^{N} Z_i(z) W_i(\omega) \mathcal{G}_i^1(G_1) \mathcal{E}_i^1(\zeta_1) \mathcal{G}_i^2(G_2) \mathcal{E}_i^2(\zeta_2) \cdots \mathcal{G}_i^\mathcal{L}(G_\mathcal{L}) \mathcal{E}_i^\mathcal{L}(\zeta_\mathcal{L}) \tag{41}$$

For constructing the separated representation (41), we proceed as just described, solving at each iteration $2 + 2\mathcal{L}$ one-dimensional problems. In the example addressed in Section 7, we consider three layers, $\mathcal{L} = 3$, which implies a parametric problem defined in eight dimensions. In this case, the use of the Proper Generalized Decomposition allows circumventing the curse of dimensionality in the calculation of the parametric solution in such a multidimensional space.

6. Non-linear solver

As described in Section 4, the equivalent linear model assumes that the shear modulus and damping ratio are functions of shear strain amplitude. Thus an iteration process is required in order to solve the resulting non-linear problem.

As shown in Fig. 4, the values of both parameters G and ζ are initialized at their small strain values, and then, after solving the dynamic problem, the maximum and effective shear strains previously defined are calculated.

Then both (the shear modulus G and the damping ratio ζ) are updated and the dynamic problem is solved again, in fact within the PGD framework, the parametric solution is particularized for the new couple of parameters. The iteration continues until reaching convergence. When the solid deposit is composed of different layers, the shear strain is calculated at each layer.

The whole solution procedure can be summarized as follows.

(i) *Offline step:* Construction of the PGD-based parametric monolayer or multilayer displacements, $\mathcal{U}(z, \omega, G, \zeta)$ and $\mathcal{U}(z, \omega, G_1, \zeta_1, G_2, \zeta_2, \cdots, G_\mathcal{L}, \zeta_\mathcal{L})$ respectively.

(ii) *Online step:* Calculation of the real-time non-linear dynamic response for a given time-dependent excitation, here assumed expressed as $\mathbf{F}(t) = \mathbf{f}g(t)$:

(a) perform the Fourier transform of the applied load

$$c(\omega) = \mathcal{F}(g(t)) \tag{42}$$

(b) make an initial estimation of shear modulus and damping ratio, G and ζ at the midpoint of each layer (assuming a linear regime, that is, small strains):

$$(G_1^0, \zeta_1^0, G_2^0, \zeta_2^0, \cdots, G_{\mathcal{L}}^0, \zeta_{\mathcal{L}}^0) \tag{43}$$

(c) repeat until convergence:
   – the response to each frequency present in the excitation can be determined from the PGD parametric solution

$$\mathcal{U}(z, \omega, G_1^m, \zeta_1^m, G_2^m, \zeta_2^m, \cdots, G_{\mathcal{L}}^m, \zeta_{\mathcal{L}}^m) \tag{44}$$

where m indicated the non-linear iteration. The total response is obtained by superposition

$$\mathcal{U}^m(z, t) = \int_{\omega^-}^{\omega^+} c(\omega)\, \mathcal{U}(z, \omega, G_1^m, \zeta_1^m, G_2^m, \zeta_2^m, \cdots, G_{\mathcal{L}}^m, \zeta_{\mathcal{L}}^m)\, \mathrm{e}^{\mathrm{i}\omega t}\, \mathrm{d}\omega \tag{45}$$

   – calculate the time evolution of the strain at the midpoint of each layer $\gamma(z_l, t)$ and from it calculate at the midpoint of each layer z_l, $l = 1, \cdots, \mathcal{L}$, the maximum strain and the corresponding effective shear strain, $\gamma_{\max}(z_l)$ and $\gamma_{\text{eff}}(z_l)$ respectively;
   – from $\gamma_{\text{eff}}(z_l)$ update at each layer the values of the shear modulus G_l^{m+1} and the damping ratio ζ_l^{m+1} using the appropriate behavior curves, as the ones illustrated in Fig. 3;
   – check convergence by defining the error E^m:

$$E^m = \sum_{l=1}^{\mathcal{L}} \left(\frac{|G_l^{m+1} - G_l^m|^2}{|G_l^1|^2} + \frac{|\zeta_l^{m+1} - \zeta_l^m|^2}{|\zeta_l^1|^2} \right) \tag{46}$$

Remark. Each "computational" layer is composed of a single material and the effective strain in it must be relatively homogeneous; both constraints serve to consider that the mechanical behavior everywhere in the latter can be represented by the one existing at the middle point. In practical applications, a few layers suffice for representing accurately a soil deposit, but this question must be carefully addressed in each particular case to conclude as regards solute convergence.

7. Numerical examples

In this section, two numerical examples for illustrating the potentialities of the technique just proposed are presented. The PGD approach was deeply compared with the solutions obtained by using the EERA software in [9]. In the first numerical simulation we consider a single clay layer with the properties illustrated in Fig. 3 ($G = 10^6$ Pa, $\zeta = 0.0048$ and $\rho = 1966$ kg/m^3), whereas in the second simulation the three layers are composed of sand ($G = 10^6$ Pa, $\zeta = 0.001$ and $\rho = 1966$ kg/m^3). In the non-linear case, both the shear modulus and the damping ratio evolve as a function of the effective strain, as previously described. In the linear case, both remain constant all along the simulation.

7.1. Soil deposit composed of a single layer

First we consider a soil deposit consisting of a single stratum. The PGD method was used to calculate the parametric solution to the displacement field $\mathcal{U}(z, \omega, G, \zeta)$. The problem's coordinates are defined in the domains $\Omega_z = (0, 1)$, $\Omega_\omega = 2\pi\,(0, 25)$ s^{-1}, $\Omega_G = (10^7, 10^8)$ Pa and $\Omega_\zeta = (0.004, 0.5)$ s^{-1}. The different domains were discretized by considering respectively 100, 1023, 1000 and 1000 nodes. Even if 1000 nodes for discretizing the parametric domains seem too much, as the calculation of functions depending on the parameters does not imply the solution to linear systems, it is preferable to consider a rich-enough discretization to be sure of representing accurately the parametric solution. The separated representation only involved five modes (the four most significant ones are depicted in Fig. 5). A detailed analysis of the solution accuracy with respect to the number of PGD modes employed and the number of nodes used for discretizing the different dimensions can be found in [6]. Fig. 6 depicts the fixed-point error evolution with respect to the PGD enrichment iterations, i.e. the error with respect to the number of PGD modes. Thus, the solution to around 5×4 one-dimensional problems for computing the five functions of the z, ω, G and ζ coordinates suffices to account for one million of scenarios (the number of nodes for discretizing the domain Ω_G times the ones involved in the discretization of Ω_ζ). Moreover, each one has a resolution of 1023 frequencies uniformly distributed in Ω_ω. The offline computing time for calculating the parametric solution was of 7 s using a standard laptop using Matlab.

Then, the response under the linear behavior assumption and the one considering its dependence with the strain amplitude were calculated using the algorithm described in the previous section. The non-linear solution only required five iterations. The computational procedure when employing the parametric solution allowed reducing by more than one order of magnitude the online computing time, from one minute to a few seconds.
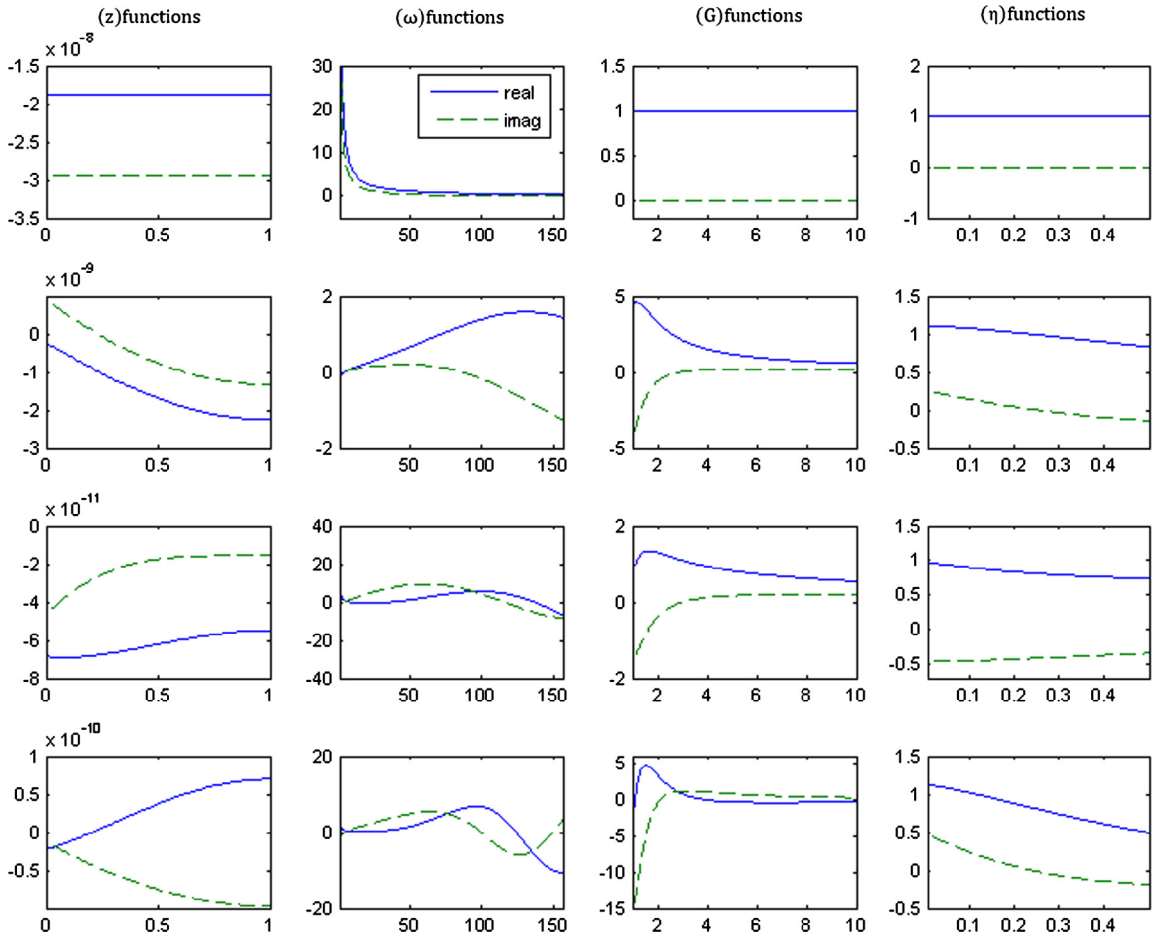
Fig. 5. First four modes involved in the separated representation of the displacement field when considering a single stratum.
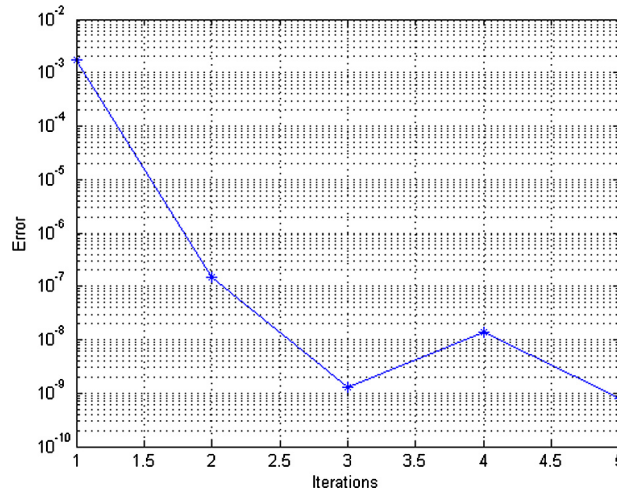

Fig. 6. Error versus number of PGD modes (iterations).

Fig. 7 shows the difference between the linear and non-linear displacement solution at the interface between the soil deposit and the elastic half-space, that is, at $z = 0$, for the given seismic excitation given in Fig. 8. Significant differences in the response can be noticed, justifying the non-linear approach, which, when using the PGD-based parametric solution, can be performed in real-time without increasing computational complexity.
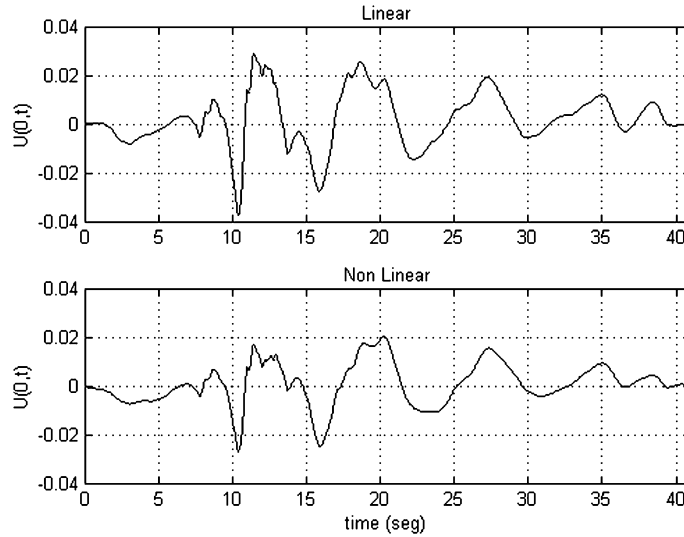
Fig. 7. Displacement versus time for linear (top) and non-linear (bottom) soil behaviors.
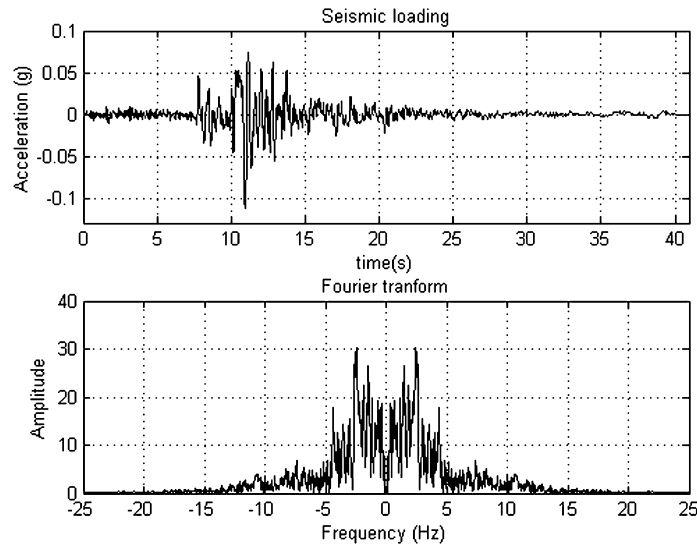

Fig. 8. Seismic loading: time (top) and frequency (bottom) representations.

7.2. Soil deposit composed of three layers

A more complex scenario consists of a soil deposit involving three strata. In this case, the PGD solution involves the space z, the frequency ω, the shear modulus of each layer G_1, G_2 and G_3, as well as the three corresponding damping ratios ζ_1, ζ_2 and ζ_3, that is, eight coordinates.

Now the domain Ω_z considered in the previous section is decomposed in three layer of thickness $L/3$. The consideration of six extra-coordinates (the shear modulus and the damping coefficient of each layer) increased the number of modes involved in the separated representation that now was of 200. In the present case, using 1000 nodes for discretizing the different domains related to the shear modulus – $\Omega_G = (10^4, 10^6)$ Pa – and the damping – $\Omega_\zeta = (0.002, 0.6)$ s^{-1} – coefficients, the obtained parametric solution is able to describe the $1000^6 = 10^{18}$ possible scenarios. We considered 600 nodes for discretizing Ω_z and again 1023 in $\Omega_\omega = (0, 157)$.

Then, the response under the linear behavior assumption and the one considering its dependence on strain amplitude were calculated using the algorithm described in the previous section. The non-linear solution only required five iterations. Again, the solution procedure when employing the parametric solution allows reducing by more than one order of magnitude the computing time, from a few minutes to a few seconds.
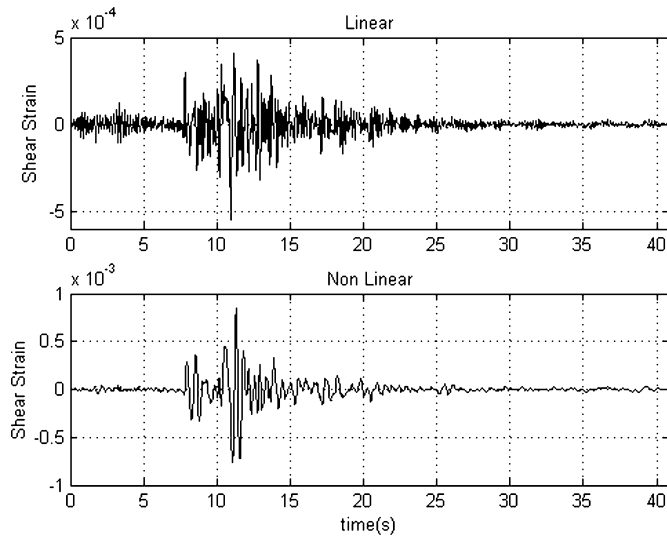
Fig. 9. Shear strain versus time at the third layer for the linear (top) and non-linear (bottom) soil behavior.
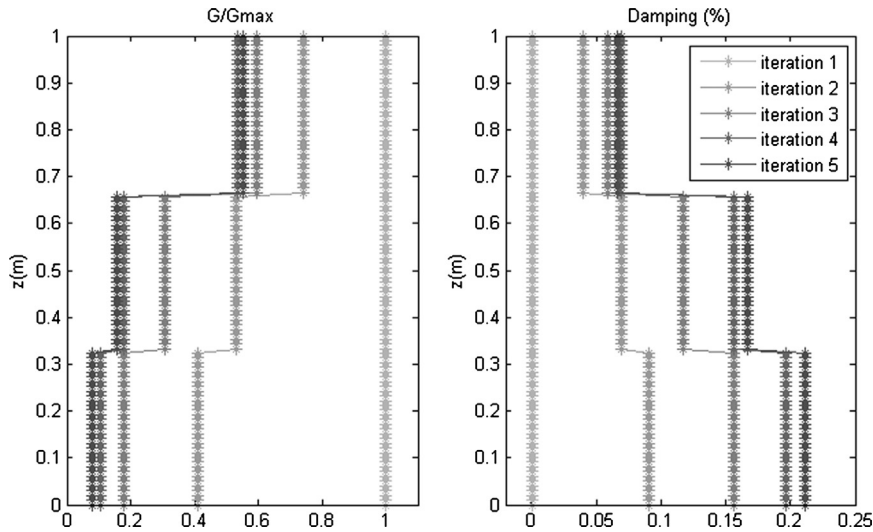

Fig. 10. $G/G_{\max}$ and damping ratio (ζ) for each layer at each iteration of the non-linear solver.

Fig. 9 illustrates the time evolution of the shear strain in the third stratum layer for both the linear and the non-linear cases, when the seismic loading represented in Fig. 8 applies. Significant differences in the response are again noticed. In the non-linear case at each iteration the shear modulus and the damping ratio at each layer are updated and the properties obtained after convergence differ from those characteristic of the linear behavior (first iteration), as reported in Fig. 10.

8. Conclusion

This paper proposes a new methodology able to compute very fast solutions to non-linear soil dynamics. The approach combines different ingredients: (i) a harmonic space-frequency description of the dynamic problem; (ii) the introduction of material parameters as model extra-coordinates, which, combined with the harmonic formulation, avoid the difficulties related to the calculation of parametric eigenproblems needed when considering usual modal-based analyses; (iii) an online integration that proceeds by particularizing the parametric solution for the material parameters, and then updating the material parameters from the just calculated solution.

More complex geometries and more complex rheological models are being considered. The first one is being addressed by considering richer parameterizations of the linearized behavior and the second by using multi-mode spring-dashpot elements with eventual fractional damping. These questions constitute a work in progress.
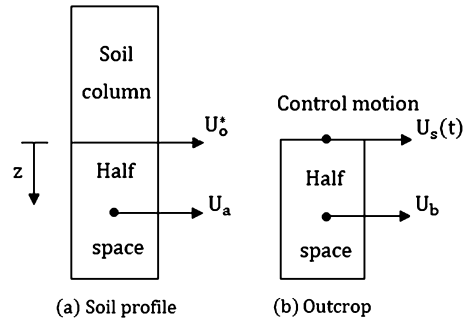
Fig. 11. Control motion at outcrop.

Appendix A. Outcropping motion analysis

The transverse displacement in the rock outcropping is produced by shear waves propagation, that results from the solution to

$$G\frac{\partial^2 U}{\partial z^2} - \rho\frac{\partial^2 U}{\partial t^2} = 0 \tag{A.1}$$

where G is the shear modulus and ρ the bedrock density.

The solution to equation (A.1) is given by

$$U = (A\,e^{ikz} + B\,e^{-ikz})e^{i\omega t} \tag{A.2}$$

where ω is the circular frequency, k the wave number, $k = \frac{\omega}{c_s}$, c_s the wave velocity ($c_s = \sqrt{\frac{G}{\rho}}$) and A and B the amplitudes of the waves propagating along the $-z$ (upward) and $+z$ (downward) directions, respectively (see Fig. 2).

Thus, the displacement U_b of points in the half-space (see Fig. 11 (right)) writes

$$U_b = (A\,e^{ikz} + B\,e^{-ikz})\,e^{i\omega t} \tag{A.3}$$

that implies the shear stress

$$\tau = G\frac{\partial U_b}{\partial z} = ikG(Ae^{ikz} - Be^{-ikz})\,e^{i\omega t} \tag{A.4}$$

At the free surface, the shear stress, and consequently the shear strain, must vanish:

$$\tau(z=0) = G\gamma(z=0) = G\left.\frac{\partial U_b}{\partial z}\right|_{z=0} = 0 \tag{A.5}$$

implying $A = B$. Thus, the surface motion reads:

$$U_s(t) = U_b(z=0,t) = 2A\,e^{i\omega t} \tag{A.6}$$

In the combined system (bedrock half-space supporting the soil deposit) illustrated in Fig. 11(a) the motion in that bedrock half-space writes now

$$U_a = (A\,e^{ikz} + B^*\,e^{-ikz})\,e^{i\omega t} \tag{A.7}$$

and the associated shear stress

$$\tau^* = G\frac{\partial U_a}{\partial z} = ikG(A\,e^{ikz} - B^*\,e^{-ikz})\,e^{i\omega t} \tag{A.8}$$

that when particularized at $z = 0$ imply

$$U_0^*(t) = U_a(z=0,t) = (A + B^*)\,e^{i\omega t} \tag{A.9}$$

and

$$\tau_0^*(t) = \tau^*(z=0,t) = ikG(A - B^*)\,e^{i\omega t} \tag{A.10}$$

that lead to

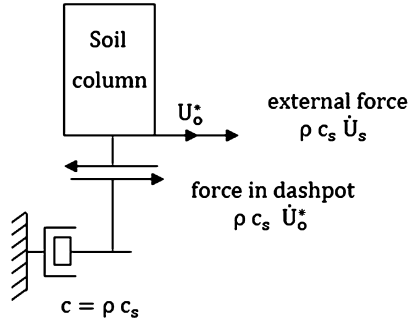$$U_0^*(t) + \frac{\tau_0^*(t)}{ikG} = 2A\,e^{i\omega t} = U_s(t) \tag{A.11}$$

Fig. 12. Half-space representation.

Therefore, from Eq. (A.11), the shear stress at the interface bedrock-soil deposit reads

$$\tau_o^* = \mathrm{i}kG(U_s - U_o^*) \tag{A.12}$$

that with $k = \frac{\omega}{c_s}$ writes

$$\tau_o^* = \mathrm{i}\frac{\omega}{c_s}G(U_s - U_o^*) \tag{A.13}$$

or making use of the relation $c_s = \sqrt{\frac{G}{\rho}}$

$$\tau_o^* = \mathrm{i}\omega\rho c_s(U_s - U_o^*) \tag{A.14}$$

Hence, the shear stress at the soil-deposit-half-space interface reads

$$\tau_o^* = \rho c_s(\dot{U}_s - \dot{U}_o^*) = \rho c_s\dot{U}_s - \rho c_s\dot{U}_o^* \tag{A.15}$$

whose first term corresponds to the measured outcropping motion and the second is like a dashpot [12]. Thus, the bedrock half-space can be substituted with boundary condition (A.15) (Fig. 12).

Appendix B. The Proper Generalized Decomposition construction

In this section the equations considered for updating the four functions involved in the displacement separated representation $Z_{n+1}(z)$, $W_{n+1}(\Omega)$, $\mathcal{G}_{n+1}(G)$ and $\mathcal{E}_{n+1}(\zeta)$ are derived.

B.1. Computing $Z_{n+1}(z)$ from $W_{n+1}(\omega)$, $\mathcal{G}_{n+1}(G)$ and $\mathcal{E}_{n+1}(\zeta)$

In this case the test function reads

$$\mathcal{U}^* = Z^*(z)W_{n+1}(\omega)\mathcal{G}_{n+1}(G)\mathcal{E}_{n+1}(\zeta) \tag{B.1}$$

Introducing equations (28) and (B.1) into (29), we get:

$$\int_{\Omega_z \times \Omega_\omega \times \Omega_G \times \Omega_\zeta} Z^* W_{n+1}\mathcal{G}_{n+1}\mathcal{E}_{n+1}\rho\omega^2 \left(\sum_{i=1}^{i=n} Z_i W_i \mathcal{G}_i \mathcal{E}_i + Z_{n+1} W_{n+1}\mathcal{G}_{n+1}\mathcal{E}_{n+1}\right) \mathrm{d}z\,\mathrm{d}\omega\,\mathrm{d}G\,\mathrm{d}\zeta$$

$$- \int_{\Omega_z \times \Omega_\omega \times \Omega_G \times \Omega_\zeta} Z^{*'} W_{n+1}\mathcal{G}_{n+1}\mathcal{E}_{n+1}\, G(1 + \mathrm{i}2\zeta) \left(\sum_{i=1}^{i=n} Z_i' W_i \mathcal{G}_i \mathcal{E}_i + Z_{n+1}' W_{n+1}\mathcal{G}_{n+1}\mathcal{E}_{n+1}\right) \mathrm{d}z\,\mathrm{d}\omega\,\mathrm{d}G\,\mathrm{d}\zeta$$

$$+ \int_{\Omega_\omega \times \Omega_G \times \Omega_\zeta} Z^*(0)W_{n+1}\mathcal{G}_{n+1}\mathcal{E}_{n+1}\mathrm{i}\rho\omega c_s \left(\sum_{i=1}^{i=n} Z_i(0) W_i \mathcal{G}_i \mathcal{E}_i + Z_{n+1}(0) W_{n+1}\mathcal{G}_{n+1}\mathcal{E}_{n+1}\right) \mathrm{d}\omega\,\mathrm{d}G\,\mathrm{d}\zeta$$

$$- \int_{\Omega_\omega \times \Omega_G \times \Omega_\zeta} Z^*(0)W_{n+1}\mathcal{G}_{n+1}\mathcal{E}_{n+1}\, \mathrm{d}\omega\,\mathrm{d}G\,\mathrm{d}\zeta = 0 \tag{B.2}$$

Integrating in $\Omega_\omega \times \Omega_G \times \Omega_\zeta$ and using the following notations:

$$
\begin{cases}
\alpha_i = \int_{\Omega_\omega \times \Omega_G \times \Omega_\zeta} W_{n+1} \mathcal{G}_{n+1} \mathcal{E}_{n+1} \rho \omega^2 W_i \mathcal{G}_i \mathcal{E}_i \ \mathrm{d}\omega \, \mathrm{d}G \, \mathrm{d}\zeta \\
\beta_i = \int_{\Omega_\omega \times \Omega_G \times \Omega_\zeta} W_{n+1} \mathcal{G}_{n+1} \mathcal{E}_{n+1} \ G(1 + \mathrm{i}2\zeta) W_i \mathcal{G}_i \mathcal{E}_i \ \mathrm{d}\omega \, \mathrm{d}G \, \mathrm{d}\zeta \\
\delta_i = \int_{\Omega_\omega \times \Omega_G \times \Omega_\zeta} W_{n+1} \mathcal{G}_{n+1} \mathcal{E}_{n+1} \rho \omega c_{\mathrm{s}} W_i \mathcal{G}_i \mathcal{E}_i \ \mathrm{d}\omega \mathrm{d}G \, \mathrm{d}\zeta \\
\gamma_1 = \int_{\Omega_\omega \times \Omega_G \times \Omega_\zeta} (W_{n+1} \mathcal{G}_{n+1} \mathcal{E}_{n+1})^2 \rho \omega^2 \ \mathrm{d}\omega \, \mathrm{d}G \, \mathrm{d}\zeta \\
\gamma_2 = \int_{\Omega_\omega \times \Omega_G \times \Omega_\zeta} (W_{n+1} \mathcal{G}_{n+1} \mathcal{E}_{n+1})^2 \ G(1 + \mathrm{i}2\zeta) \ \mathrm{d}\omega \, \mathrm{d}G \, \mathrm{d}\zeta \\
\phi_1 = \int_{\Omega_\omega \times \Omega_G \times \Omega_\zeta} W_{n+1} \mathcal{G}_{n+1} \mathcal{E}_{n+1} \, \mathrm{d}\omega \, \mathrm{d}G \, \mathrm{d}\zeta \\
\phi_2 = \int_{\Omega_\omega \times \Omega_G \times \Omega_\zeta} (W_{n+1} \mathcal{G}_{n+1} \mathcal{E}_{n+1})^2 \rho \omega c_{\mathrm{s}} \ \mathrm{d}\omega \mathrm{d}G \, \mathrm{d}\zeta
\end{cases} \tag{B.3}
$$

it results:

$$
\int_{\Omega_z} Z^* \gamma_1 Z_{n+1} \, \mathrm{d}z + \int_{\Omega_z} Z^* \sum_{i=1}^{i=n} \alpha_i Z_i \, \mathrm{d}z - \int_{\Omega_z} Z^{*'} \sum_{i=1}^{i=n} \beta_i Z_i' \, \mathrm{d}z - \int_{\Omega_z} Z^{*'} \gamma_2 Z_{n+1}' \, \mathrm{d}z
$$
$$
+ Z^*(0) \sum_{i=1}^{i=n} \mathrm{i}\delta_i Z_i(0) + Z^*(0)\mathrm{i}\phi_2 Z_{n+1}(0) - Z^*(0)\phi_1 = 0 \tag{B.4}
$$

or, by integrating by parts,

$$
\int_{\Omega_z} Z^* \gamma_1 Z_{n+1} \, \mathrm{d}z - \int_{\Omega_z} Z^{*'} \gamma_2 Z_{n+1}' \, \mathrm{d}z + \int_{\Omega_z} Z^* \left(\sum_{i=1}^{i=n} \alpha_i Z_i + \beta_i Z_i'' \right) \mathrm{d}z
$$
$$
+ Z^*(0) \sum_{i=1}^{i=n} \left(\beta_i Z_i'(0) + Z_i(0)\mathrm{i}\delta_i \right) - Z^*(0)\phi_1 + Z^*(0)\mathrm{i}\phi_2 Z_{n+1}(0) = 0 \tag{B.5}
$$

Observe that integrals defined in Eq. (B.3) can be computed easily as the product of one-dimensional integrals defined on Ω_ω, Ω_G and Ω_ζ, respectively, thanks to the separated representation of the functions.

B.2. Computing $W_{n+1}(\omega)$ from $Z_{n+1}(z)$, $\mathcal{G}_{n+1}(G)$ and $\mathcal{E}_{n+1}(\zeta)$

Now the test function reads

$$
\mathcal{U}^* = Z_{n+1}(z) W^*(\omega) \mathcal{G}_{n+1}(G) \, \mathcal{E}_{n+1}(\zeta) \tag{B.6}
$$

and the problem weak form becomes

$$
\int_{\Omega_z \times \Omega_\omega \times \Omega_G \times \Omega_\zeta} Z_{n+1} W^* \mathcal{G}_{n+1} \mathcal{E}_{n+1} \rho \omega^2 \left(\sum_{i=1}^{i=n} Z_i W_i \mathcal{G}_i \mathcal{E}_i + Z_{n+1} W_{n+1} \mathcal{G}_{n+1} \mathcal{E}_{n+1} \right) \mathrm{d}z \, \mathrm{d}\omega \, \mathrm{d}G \, \mathrm{d}\zeta
$$
$$
- \int_{\Omega_z \times \Omega_\omega \times \Omega_G \times \Omega_\zeta} Z_{n+1}' W^* \mathcal{G}_{n+1} \mathcal{E}_{n+1} \ G(1 + \mathrm{i}2\zeta) \left(\sum_{i=1}^{i=n} Z_i' W_i \mathcal{G}_i \mathcal{E}_i + Z_{n+1}' W_{n+1} \mathcal{G}_{n+1} \mathcal{E}_{n+1} \right) \mathrm{d}z \, \mathrm{d}\omega \, \mathrm{d}G \, \mathrm{d}\zeta
$$
$$
+ \int_{\Omega_\omega \times \Omega_G \times \Omega_\zeta} Z_{n+1}(0) W^* \mathcal{G}_{n+1} \mathcal{E}_{n+1} \mathrm{i}\rho \omega c_{\mathrm{s}} \left(\sum_{i=1}^{i=n} Z_i(0) W_i \mathcal{G}_i \mathcal{E}_i + Z_{n+1}(0) W_{n+1} \mathcal{G}_{n+1} \mathcal{E}_{n+1} \right) \mathrm{d}\omega \, \mathrm{d}G \, \mathrm{d}\zeta
$$
$$
- \int_{\Omega_\omega \times \Omega_G \times \Omega_\zeta} Z_{n+1}(0) W^* \mathcal{G}_{n+1} \mathcal{E}_{n+1} \ \mathrm{d}\omega \, \mathrm{d}G \, \mathrm{d}\zeta = 0 \tag{B.7}
$$

Integrating in $\Omega_z \times \Omega_G \times \Omega_\zeta$ and taking into account the expressions:

$$
\begin{cases}
\alpha_i = \int_{\Omega_z \times \Omega_G \times \Omega_\zeta} Z_{n+1} \mathcal{G}_{n+1} \mathcal{E}_{n+1} \rho Z_i \mathcal{G}_i \mathcal{E}_i \ \mathrm{d}z \, \mathrm{d}G \, \mathrm{d}\zeta \\
\beta_i = \int_{\Omega_z \times \Omega_G \times \Omega_\zeta} Z'_{n+1} \mathcal{G}_{n+1} \mathcal{E}_{n+1} \ G(1 + \mathrm{i}2\zeta) Z'_i \mathcal{G}_i \mathcal{E}_i \ \mathrm{d}z \, \mathrm{d}G \, \mathrm{d}\zeta \\
\delta_i = \int_{\Omega_G \times \Omega_\zeta} \mathcal{G}_{n+1} \mathcal{E}_{n+1} \rho c_\mathrm{s} \mathcal{G}_i \mathcal{E}_i \ \mathrm{d}G \, \mathrm{d}\zeta \\
\gamma_1 = \int_{\Omega_z \times \Omega_G \times \Omega_\zeta} (Z_{n+1} \mathcal{G}_{n+1} \mathcal{E}_{n+1})^2 \rho \ \mathrm{d}z \, \mathrm{d}G \, \mathrm{d}\zeta \\
\gamma_2 = \int_{\Omega_z \times \Omega_G \times \Omega_\zeta} (Z'_{n+1} \mathcal{G}_{n+1} \mathcal{E}_{n+1})^2 \ G(1 + \mathrm{i}2\zeta) \ \mathrm{d}z \, \mathrm{d}G \, \mathrm{d}\zeta \\
\phi_1 = \int_{\Omega_G \times \Omega_\zeta} \mathcal{G}_{n+1} \mathcal{E}_{n+1} \, \mathrm{d}G \, \mathrm{d}\zeta \\
\phi_2 = \int_{\Omega_G \times \Omega_\zeta} (\mathcal{G}_{n+1} \mathcal{E}_{n+1})^2 \rho c_\mathrm{s} \, \mathrm{d}G \, \mathrm{d}\zeta
\end{cases}
\tag{B.8}
$$

it results

$$
\int_{\Omega_\omega} W^* (\gamma_1 \omega^2 - \gamma_2 + \mathrm{i}\omega \phi_2 Z_{n+1}^2(0)) W_{n+1} \, \mathrm{d}\omega
$$

$$
+ \int_{\Omega_\omega} W^* \left[-\phi_1 Z_{n+1}(0) + \sum_{i=1}^{i=n} (\alpha_i \omega^2 - \beta_i + \mathrm{i}\omega Z_i(0) Z_{n+1}(0) \delta_i) W_i \right] \mathrm{d}\omega = 0
\tag{B.9}
$$

whose strong form reads

$$
W_{n+1} = \frac{\phi_1 Z_{n+1}(0) + \sum_{i=1}^{i=n} \left(\beta_i - \alpha_i \omega^2 - \mathrm{i}\omega Z_i(0) Z_{n+1}(0) \delta_i \right) W_i}{\gamma_1 \omega^2 - \gamma_2 + \mathrm{i}\omega \phi_2 Z_{n+1}^2(0)}
\tag{B.10}
$$

B.3. Computing $\mathcal{G}_{n+1}(G)$ from $Z_{n+1}(z)$, $W_{n+1}(\omega)$ and $\mathcal{E}_{n+1}(\zeta)$

Now, with the test function given by:

$$
\mathcal{U}^* = Z_{n+1}(z) W_{n+1}(\omega) \mathcal{G}^*(G) \mathcal{E}_{n+1}(\zeta)
\tag{B.11}
$$

the weak form reads:

$$
\int_{\Omega_z \times \Omega_\omega \times \Omega_G \times \Omega_\zeta} Z_{n+1} W_{n+1} \mathcal{G}^* \mathcal{E}_{n+1} \rho \omega^2 \left(\sum_{i=1}^{i=n} Z_i W_i \mathcal{G}_i \mathcal{E}_i + Z_{n+1} W_{n+1} \mathcal{G}_{n+1} \mathcal{E}_{n+1} \right) \mathrm{d}z \, \mathrm{d}\omega \, \mathrm{d}G \, \mathrm{d}\zeta
$$

$$
- \int_{\Omega_z \times \Omega_\omega \times \Omega_G \times \Omega_\zeta} Z'_{n+1} W_{n+1} \mathcal{G}^* \mathcal{E}_{n+1} \ G(1 + \mathrm{i}2\zeta) \left(\sum_{i=1}^{i=n} Z'_i W_i \mathcal{G}_i \mathcal{E}_i + Z'_{n+1} W_{n+1} \mathcal{G}_{n+1} \mathcal{E}_{n+1} \right) \mathrm{d}z \, \mathrm{d}\omega \, \mathrm{d}G \, \mathrm{d}\zeta
$$

$$
+ \int_{\Omega_\omega \times \Omega_G \times \Omega_\zeta} Z_{n+1}(0) W_{n+1} \mathcal{G}^* \mathcal{E}_{n+1} \mathrm{i}\rho \omega c_\mathrm{s} \left(\sum_{i=1}^{i=n} Z_i(0) W_i \mathcal{G}_i \mathcal{E}_i + Z_{n+1}(0) W_{n+1} \mathcal{G}_{n+1} \mathcal{E}_{n+1} \right) \mathrm{d}\omega \, \mathrm{d}G \, \mathrm{d}\zeta
$$

$$
- \int_{\Omega_\omega \times \Omega_G \times \Omega_\zeta} Z_{n+1}(0) W_{n+1} \mathcal{G}^* \mathcal{E}_{n+1} \ \mathrm{d}\omega \, \mathrm{d}G \, \mathrm{d}\zeta = 0
\tag{B.12}
$$

Integrating in $\Omega_z \times \Omega_\omega \times \Omega_\zeta$ and taking into account:

$$
\begin{cases}
\alpha_i = \int_{\Omega_z \times \Omega_\omega \times \Omega_\zeta} Z_{n+1} W_{n+1} \mathcal{E}_{n+1} \rho \omega^2 Z_i W_i \mathcal{E}_i \ \mathrm{d}z \, \mathrm{d}\omega \, \mathrm{d}\zeta \\
\beta_i = \int_{\Omega_z \times \Omega_\omega \times \Omega_\zeta} Z'_{n+1} W_{n+1} \mathcal{E}_{n+1} \ (1 + \mathrm{i}2\zeta) Z'_i W_i \mathcal{E}_i \ \mathrm{d}z \, \mathrm{d}\omega \, \mathrm{d}\zeta \\
\delta_i = \int_{\Omega_\omega \times \Omega_\zeta} W_{n+1} \mathcal{E}_{n+1} \rho c_\mathrm{s} \omega W_i \mathcal{E}_i \ \mathrm{d}\omega \, \mathrm{d}\zeta \\
\gamma_1 = \int_{\Omega_z \times \Omega_\omega \times \Omega_\zeta} (Z_{n+1} W_{n+1} \mathcal{E}_{n+1})^2 \rho \omega^2 \ \mathrm{d}z \, \mathrm{d}\omega \, \mathrm{d}\zeta \\
\gamma_2 = \int_{\Omega_z \times \Omega_\omega \times \Omega_\zeta} (Z'_{n+1} W_{n+1} \mathcal{E}_{n+1})^2 \ (1 + \mathrm{i}2\zeta) \ \mathrm{d}z \, \mathrm{d}\omega \, \mathrm{d}\zeta \\
\phi_1 = \int_{\Omega_\omega \times \Omega_\zeta} W_{n+1} \mathcal{E}_{n+1} \ \mathrm{d}\omega \, \mathrm{d}\zeta \\
\phi_2 = \int_{\Omega_\omega \times \Omega_\zeta} (W_{n+1} \mathcal{E}_{n+1})^2 \rho c_\mathrm{s} \omega \ \mathrm{d}\omega \, \mathrm{d}\zeta
\end{cases}
\tag{B.13}
$$

the weak form writes

$$\int\limits_{\Omega_G} \mathcal{G}^* \left(\gamma_1 - G\gamma_2 + \mathrm{i}\phi_2 Z_{n+1}^2(0) \right) \mathcal{G}_{n+1}\mathrm{d}G$$

$$+ \int\limits_{\Omega_G} \mathcal{G}^* \left[-\phi_1 Z_{n+1}(0) + \sum_{i=1}^{i=n} (\alpha_i - \beta_i G + \mathrm{i}Z_i(0)Z_{n+1}(0)\delta_i)\,\mathcal{G}_i \right] \mathrm{d}G = 0 \tag{B.14}$$

whose associated strong form reads

$$\mathcal{G}_{n+1} = \frac{\phi_1 Z_{n+1}(0) + \sum_{i=1}^{i=n} (\beta_i G - \alpha_i - \mathrm{i}Z_i(0)Z_{n+1}(0)\delta_i)\,\mathcal{G}_i}{\gamma_1 - G\gamma_2 + \mathrm{i}\phi_2 Z_{n+1}^2(0)} \tag{B.15}$$

B.4. Computing $\mathcal{E}(\zeta)$ from $Z_{n+1}(z)$, $W_{n+1}(\omega)$ and $\mathcal{G}_{n+1}(G)$

Finally, with

$$\mathcal{U}^* = Z_{n+1}(z)W_{n+1}(\omega)\mathcal{G}_{n+1}(G)\mathcal{E}^*(\zeta) \tag{B.16}$$

the weak form reads:

$$\int\limits_{\Omega_z \times \Omega_\omega \times \Omega_G \times \Omega_\zeta} Z_{n+1}W_{n+1}\mathcal{G}_{n+1}\mathcal{E}^*\rho\omega^2 \left(\sum_{i=1}^{i=n} Z_iW_i\mathcal{G}_i\mathcal{E}_i + Z_{n+1}W_{n+1}\mathcal{G}_{n+1}\mathcal{E}_{n+1} \right) \mathrm{d}z\,\mathrm{d}\omega\,\mathrm{d}G\,\mathrm{d}\zeta$$

$$- \int\limits_{\Omega_z \times \Omega_\omega \times \Omega_G \times \Omega_\zeta} Z_{n+1}'W_{n+1}\mathcal{G}_{n+1}\mathcal{E}^*\,G(1+\mathrm{i}2\zeta) \left(\sum_{i=1}^{i=n} Z_i'W_i\mathcal{G}_i\mathcal{E}_i + Z_{n+1}'W_{n+1}\mathcal{G}_{n+1}\mathcal{E}_{n+1} \right) \mathrm{d}z\,\mathrm{d}\omega\,\mathrm{d}G\,\mathrm{d}\zeta$$

$$+ \int\limits_{\Omega_\omega \times \Omega_G \times \Omega_\zeta} Z_{n+1}(0)W_{n+1}\mathcal{G}_{n+1}\mathcal{E}^*\mathrm{i}\rho\omega c_\mathrm{s} \left(\sum_{i=1}^{i=n} Z_i(0)W_i\mathcal{G}_i\mathcal{E}_i + Z_{n+1}(0)W_{n+1}\mathcal{G}_{n+1}\mathcal{E}_{n+1} \right) \mathrm{d}\omega\,\mathrm{d}G\,\mathrm{d}\zeta$$

$$- \int\limits_{\Omega_\omega \times \Omega_G \times \Omega_\zeta} Z_{n+1}(0)W_{n+1}\mathcal{G}_{n+1}\mathcal{E}^*\,\mathrm{d}\omega\,\mathrm{d}G\,\mathrm{d}\zeta = 0 \tag{B.17}$$

that integrating in $\Omega_z \times \Omega_\omega \times \Omega_G$ and considering the expressions

$$\begin{cases} \alpha_i = \int_{\Omega_z \times \Omega_\omega \times \Omega_G} Z_{n+1}W_{n+1}\mathcal{G}_{n+1}\rho\omega^2 Z_iW_i\mathcal{G}_i \ \mathrm{d}z\,\mathrm{d}\omega\,\mathrm{d}G \\ \beta_i = \int_{\Omega_z \times \Omega_\omega \times \Omega_G} Z_{n+1}'W_{n+1}\mathcal{G}_{n+1}\ GZ_i'W_i\mathcal{G}_i \ \mathrm{d}z\,\mathrm{d}\omega\,\mathrm{d}G \\ \delta_i = \int_{\Omega_\omega \times \Omega_G} W_{n+1}\mathcal{G}_{n+1}\rho\omega c_\mathrm{s}W_i\mathcal{G}_i \ \mathrm{d}\omega\,\mathrm{d}G \\ \gamma_1 = \int_{\Omega_z \times \Omega_\omega \times \Omega_G} (Z_{n+1}W_{n+1}\mathcal{G}_{n+1})^2 \rho\omega^2 \ \mathrm{d}z\,\mathrm{d}\omega\,\mathrm{d}G \\ \gamma_2 = \int_{\Omega_z \times \Omega_\omega \times \Omega_G} (Z_{n+1}'W_{n+1}\mathcal{G}_{n+1})^2\ G \ \mathrm{d}z\,\mathrm{d}\omega\,\mathrm{d}G \\ \phi_1 = \int_{\Omega_\omega \times \Omega_G} W_{n+1}\mathcal{G}_{n+1} \ \mathrm{d}\omega\,\mathrm{d}G \\ \phi_2 = \int_{\Omega_\omega \times \Omega_G} (W_{n+1}\mathcal{G}_{n+1})^2 \rho\omega c_\mathrm{s} \ \mathrm{d}\omega\,\mathrm{d}G \end{cases} \tag{B.18}$$

results

$$\int\limits_{\Omega_\zeta} \mathcal{E}^*(\gamma_1 - (1+\mathrm{i}2\zeta)\gamma_2 + \mathrm{i}\phi_2 Z_{n+1}^2(0))\mathcal{E}_{n+1}\,\mathrm{d}\zeta$$

$$+ \int\limits_{\Omega_\zeta} \mathcal{E}^* \left[-\phi_1 Z_{n+1}(0) + \sum_{i=1}^{i=n} (\alpha_i - \beta_i(1+\mathrm{i}2\zeta) + \mathrm{i}Z_i(0)Z_{n+1}(0)\delta_i)\mathcal{E}_i \right] \mathrm{d}\zeta = 0$$

$$\tag{B.19}$$

or

$$\mathcal{E}_{n+1} = \frac{\phi_1 Z_{n+1}(0) + \sum_{i=1}^{i=n} (\beta_i(1+\mathrm{i}2\zeta) - \alpha_i - \mathrm{i}Z_i(0)Z_{n+1}(0)\delta_i)\,\mathcal{E}_i}{\gamma_1 - (1+\mathrm{i}2\zeta)\gamma_2 + \mathrm{i}\phi_2 Z_{n+1}^2(0)} \tag{B.20}$$

References

[1] J.-P. Bradet, K. Ichii, C.H. Lin, EERA: a computer program for equivalent-linear earthquake site response analyses of layered soil deposits, University of Southern California, Department of Civil Engineering, 2000.

[2] Y. Bozorgnia, V.V. Bertero, Earthquake Engineering: From Engineering Seismology to Performance-based Engineering, CRC Press, Boca Raton, FL, USA, 2004, pp. 415–421.

[3] F. Chinesta, P. Ladeveze, E. Cueto, A short review on model order reduction based on Proper Generalized Decomposition, Arch. Comput. Methods Eng. 18 (2011) 395–404.

[4] F. Chinesta, A. Ammar, E. Cueto, Recent advances and new challenges in the use of the Proper Generalized Decomposition for solving multidimensional models, Arch. Comput. Methods Eng. 17 (4) (2010) 327–350.

[5] F. Chinesta, A. Leygue, F. Bordeu, J.V. Aguado, E. Cueto, D. Gonzalez, I. Alfaro, Parametric PGD based computational vademecum for efficient design, optimization and control, Arch. Comput. Methods Eng. 20 (1) (2013) 31–59.

[6] F. Chinesta, R. Keunings, A. Leygue, The Proper Generalized Decomposition for Advanced Numerical Simulations. A Primer, Springerbriefs, Springer, 2014.

[7] R.W. Clough, J. Penzien, Dynamics of Structures, Civil Engineering Series, McGraw-Hill, New York, NY, 1993.

[8] S.H. Crandall, The role of damping in vibration theory, J. Sound Vib. 11 (1) (1970) 3–18.

[9] C. Germoso, Respuesta sísmica de terrenos estratificados. Comportamiento no lineal, Master Thesis, Universidad politécnica de Madrid, Madrid, Spain, 2012.

[10] K. Ishihara, N. Yoshida, S. Tsujino, Modeling of stress–strain relations of soils in cyclic loading, in: Proc. Fifth International Conference on Numerical Methods in Geomechanics, vol. 1, 1985, pp. 373–380.

[11] W.B. Joyner, A.T. Chen, Calculation of nonlinear ground response in earthquakes, Bull. Seismol. Soc. Amer. 65 (5) (1975) 1315–1336.

[12] J. Lysmer, A.M. Kuhlemeyer, Finite dynamics model for infinite media, J. Eng. Mech. 95 (1969) 859–877.

[13] Y. Murono, Y. Nogami, Shear stress-shear strain relationship taking into account S-shape hysteresis loop, in: Proc. 12th Japan Earthquake Engineering Symposium, vol. 12, 2006, pp. 494–497.

[14] A. Nishimura, Y. Murono, Nonlinear hysteresis model using GHE model and modified Masing's rule, in: Proc. JSCE Earthquake Engineering Symposium, vol. 25-1, 1999, pp. 309–312.

[15] A. Pecker, Dynamique des sols, Presses de l'école nationale des ponts et chaussées, Paris, 1984.

[16] S. Quraishi, C. Schroder, V. Mehrmann, Solution of large scale parametric eigenvalue problems arising from brake squeal modeling, Proc. Appl. Math. Mech. 14 (2014) 891–892.

[17] P.B. Schnabel, J. Lysmer, H.B. Seed, SHAKE-91: equivalent linear seismic response analysis of horizontally layered soil deposits, the earthquake engineering online archive NISEE e-library, http://nisee.berkeley.edu/elibrary/Software/SHAKE91ZIP.

[18] F. Tisseur, K. Meerbergen, The quadratic eigenvalue problem, SIAM Rev. 43 (2) (2001) 235–286.